Talanta 117 (2013) 449–455

Contents lists available at ScienceDirect

Talanta

journal homepage: www.elsevier.com/locate/talanta

Preparation of graphene oxide–silver nanoparticle nanohybrids with highly antibacterial capability

Zhijun Zhu [a,b], Min Su [a,b], Lan Ma [a,b], Lina Ma [a,*], Dianjun Liu [a], Zhenxin Wang [a,*]

[a] State Key Laboratory of Electroanalytical Chemistry, Changchun Institute of Applied Chemistry, Chinese Academy of Sciences, Changchun 130022, PR China
[b] University of the Chinese Academy of Sciences, Beijing 100049, PR China

ARTICLE INFO

Article history:
Received 3 August 2013
Received in revised form
5 September 2013
Accepted 11 September 2013
Available online 3 October 2013

Keywords:
Graphene oxide
Silver nanoparticle
PDDA
High stability
Enhanced antibacterial capability

ABSTRACT

A simple method based on electrostatic interactions was utilized to assemble silver nanoparticles (AgNPs) to graphene oxide (GO) sheets. This method allows conjugation of AgNPs with desired morphologies (densities, sizes and shapes) onto GO. In this process, poly(diallyldimethylammonium chloride) (PDDA) was introduced as an adhesive agent. The as-prepared graphene oxide–AgNPs composites (GO–AgNPs) have enhanced colloid stability and photo-stability than that of AgNPs. After conjugating to GO sheets, the antibacterial activities of AgNPs against Gram negative (G−) bacterial strain (*Escherichia coli, E. coli*) and Gram positive (G+) bacterial strain (*Bacillus subtilis, B. subtilis*) have been improved significantly. The antibacterial activity of GO–AgNPs is dependent on the size of AgNPs, i.e. the small AgNPs modified GO sheets show more effective antibacterial capability than that of large AgNPs modified GO sheets. Compared with AgNPs, the enhanced antibacterial activity of GO–AgNPs might not only be due to high stability of AgNPs anchored on GO sheets, but also the positive charged surface of hybrids which increases the electrostatic interaction of bacterial cell membrane with nanohybrids.

1. Introduction

Bacterial species have been identified as important pathogens in many severe pathogen-related diseases among humans. And bacterial pathogens are enabling to distribute in a wide range of substrates, such as soil, contaminated food and animals excrements [1–4]. One of the most effective strategies for the prevention of microbial colonization is to develop a functional material with highly antimicrobial property. Recently, the antimicrobial efficacy of engineered nanoparticles (NPs) including metal and carbon-based NPs has been widely studied [5–8]. Among the great variety of antibacterial materials, silver NPs (AgNPs) are marked out as antimicrobial reagents with high capability due to their large surface area and slow release properties [9–12]. Although the bactericidal mechanism of AgNPs is not fully understood, three possible mechanisms are usually proposed: (i) gradual release of silver ions, which can affect on DNA replication and ATP production, (ii) direct damage to cellular membranes by AgNPs, or (iii) generation of reactive oxygen species (ROS) from AgNPs and Ag^+ [13]. It is believed that good dispersion of AgNPs is required for effective antibacterial activities [14]. However, colloidal AgNPs have a tendency to aggregate in practical applications due to colloidal instability, leading to deterioration of antibacterial performance [14]. Therefore, development of stable, dispersed AgNPs substrates is a critical challenge of AgNP-based antimicrobial materials because of the poorly colloidal stability of AgNPs [15–17]. To address this problem, loading AgNPs on supporting matrix is one of the most efficient strategies [17].

Graphene is a one-atom thick and two-dimensional carbon allotrope made up of a conjugated system of sp^2 carbons arranged in a honeycomb structure. It has attracted great attention and shown great potential applications for fabricating electronic devices, nanocomposites, sensors and nanocarriers [18]. Graphene oxide (GO) is strongly hydrophilic material, and easily forms stable colloidal dispersions in water because it has a great deal of oxygen bonds in its edges and defect sites, such as hydroxyl (C3OH), carboxylic (–COOH), carbonyl (C=O), epoxide groups (C3O3C) on both accessible sides [19]. The functional groups have been confirmed to be reducibility and have been actively used to build new composites [20–22]. For instance, we have synthesized a kind of thionin-bridged graphene–gold NP nanohybrids with efficient photothermal therapy ability through formation of amide bonds [23]. Cui and coauthors have used GO and AgNPs to prepare carbon nanoscrolls via several hours ultrasonic vibration, which exhibited enhanced antifungal activities [24].

In situ synthesis of GO–AgNPs with good antibacterial activity has been extensively reported [25,26]. For example, Tang and co-workers have in situ synthesized of a kind of Ag–polydopamine–graphene nanosheets as antibacterial agents [27]. However, the reduction of GO usually has a side effect on the dispersity and stability of GO–AgNPs [28] and the negative surface charge would

* Corresponding authors. Fax: +86 431 85262243.
E-mail addresses: malina@ciac.ac.cn (L. Ma), wangzx@ciac.ac.cn (Z. Wang).

0039-9140/$ - see front matter © 2013 Elsevier B.V. All rights reserved.
http://dx.doi.org/10.1016/j.talanta.2013.09.017

weaken the contact between bacterial cells and the GO–Ag nanocomposites [25]. Self-assembly is another effective method to fabricate GO–NPs nanohybrids, in this approach NPs can be prepared as requirement and GO could be used as a supporting matrix without reduction [29].

Herein, a facile method to assemble AgNPs and GO sheets is demonstrated. In this process, poly(diallyldimethylammonium chloride) (PDDA) was employed as a linker for conjugating AgNPs to GO sheets. AgNPs with different densities, sizes and shapes can be loaded onto GO sheets easily in this way. The antibacterial activities of GO–AgNPs have been investigated using Gram-negative (G-) bacteria *Escherichia coli* (*E. coli*) and Gram-positive (G+) bacteria *Bacillus subtilis* (*B. subtilis*) as model bacteria. The effects of various AgNPs sizes, mass ratio of Ag to GO–PDDA and dosages on antibacterial activity of GO–AgNPs have been examined.

2. Experimental section

2.1. Materials

Graphite was purchased from Alfa Aesar co., Ltd. (USA). Poly (diallyldimethylammonium chloride) (PDDA, 35 wt% in water) was obtained purchased from Sigma-Aldrich co., Ltd. (USA). *E. coli* (ATCC BL21) bacterial strain and *B. subtilis* (ATCC 31785) were purchased from Dingguo co., Ltd. (Beijing, China). Tryptone and yeast extract were obtained from Oxoid Co., Ltd. (England). Baird-Parker agar base was purchased from Qingdao Hope Bio-Technology Co., Ltd. (Qingdao, China). Ascorbic acid, trisodium citrate, silver nitrate ($AgNO_3$) and other agents were purchased from Beijing Chemical Reagents Co., Ltd. (Beijing, China). All reagents were analytical grade and used as received without further purification. Milli-Q water (18.2 MΩ cm) was used in all experiments.

2.2. Apparatus

UV–vis–NIR spectra were obtained by TU-1901 UV–vis–NIR spectrophotometer (Purkinje General Instrument Co., Ltd. China). FTIR characterization was carried out on Vertex70 Fourier transform infrared spectroscope (Bruker Co., Ltd. Germany). X-ray photoelectron spectroscopy (XPS) measurements were carried out on EscA-LABMK II X-ray photoelectron spectroscope (VG Scientific Co., Ltd., UK). Raman spectra were obtained by a Renishaw 2000 Raman spectrophotometer (Gloucestershire, UK) equipped with an Ar^+ ion laser (514.5 nm wavelength) and a CCD detector. Transmission electron microscopy (TEM) measurements were made on H600 Transmission electron microscope (Hitachi Co,. Ltd. Japan) with an accelerating voltage of 100 kV. The composition of the sample was determined by iCAP 6300 inductively coupled plasma-optical emission spectrometer (ICP-OES, Thermo., USA). Zeta potential measurements were made on ZEN3600 Zetasizer (Malvern Co., Ltd. UK). Thermo-gravimetric analysis (TGA) of sample was performed on a Pyris Diamond TG/DTA thermogravimetric analyzer (Perkin-Elmer Co,. Ltd. USA). In TGA experiment, the samples were heated from room temperature to 900 °C at 10 °C min^{-1} under an air atmosphere [27,30].

2.3. Synthesis of silver nanoparticle–graphene oxide

GO was prepared from natural graphite powder by the modified Hummers method [31]. Silver nanoparticles (AgNPs) with ca. 14 nm were prepared according to previous report with modification [32]. In a typical synthesis, 48 mL water was mixed with 5 mg of ascorbic acid and 40 mg of sodium citrate, and the pH of solution was adjusted to 11 with 0.2 M NaOH. 2 mL of $AgNO_3$ solution (10 mg) was added dropwise on ice-water bath. After stirred for 30 min, the solution was transferred into a 100 °C water bath for 1 h. About 46 nm AgNPs were prepared using citrate reduction method of Lee and Meisel [33]. Typically, 50 μL of 0.2 mM ascorbic acid was added into 50 mL of boiling water. 10 mg of sodium citrate and 2.5 mg of $AgNO_3$ were mixed in 3 mL of water under stirring at room temperature. After 5 min incubation at room temperature, the mixture solution was injected into the ascorbic acid solution. The solution was further boiled and stirred for 1 h and cooled down to room temperature. Ag nanoplates were prepared according to previous report [34]. Generally, 1 mg of $AgNO_3$, 26 mg of sodium citrate and 60 μL of H_2O_2 (30 wt%) were added into 50 mL of water under stirring. After stirred for 1 min, 250 μL of $NaBH_4$ (1.4 mg) was injected into the solution rapidly, and the blue colored solution indicated formation of Ag nanoplates. All of the products were stored at 4 °C for further use.

2 mL of as-prepared GO (3.0 mg mL^{-1}) was mixed with 1.6 mL of PDDA (10 mg mL^{-1}). The pH value of mixture was adjusted from 1.0 to 6.5 by 1.0 M NaOH solution under ultrasonic vibration. After ultrasonic vibration for 20 min, the mixture was centrifuged (13000 rpm, 10 min) for 3 times to remove excess PDDA. The obtained product, named as GO–PDDA, was dispersed in 10 mL water and stored at 4 °C. 100 μL of GO–PDDA was mixed with various volumes (12 mL, 6 mL, 2 mL, 670 μL or 200 μL) of AgNPs (120 μg/mL) (or 8 mL of as-prepared large AgNPs (30 μg/mL) or 15 mL of Ag nanoplates (12 μg/mL)) under ultrasonic vibration, respectively. The mixture was centrifuged (5000 rpm, 10 min) for 3 times after ultrasonic vibration for 1 min, and then the precipitate was re-dispersed in water, named as GO–AgNPs. For antibacterial test, the amounts of Ag in AgNPs and GO–AgNPs solutions were determined by ICP analysis.

2.4. Zeta potential measurement

For zeta potential measurements, 800 μL of samples dispersed in 20 mM HEPES (pH=7.4) were injected into the measuring cell. After equilibration at 25 °C for 120 s, the potential data were collected for 3 times.

2.5. Bacteria culturing

All bacterial strains were cultured in Luria-Bertani (LB) culture medium (10 g•L^{-1} tryptone, 5 g L^{-1} yeast extract, 5 g L^{-1} NaCl). The bacteria strains were incubated in LB medium with shaking at 37 °C. The optical density at 600 nm (OD_{600}) was measured to monitor bacterial growth. When the cultures reached an OD_{600} of 0.3 (the beginning of logarithmic phase) [35], the log phased strains were centrifuged at 5000 g for 8 min, and resuspended in

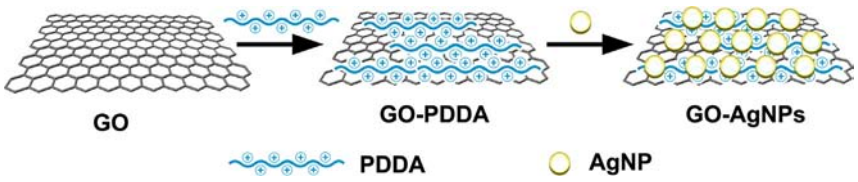

Scheme 1. Procedure for the self-assembly of AgNPs and PDDA onto GO nanosheets.

PBS [36]. In all experiments, the concentrations of bacteria were determined by OD_{600} (1 $OD_{600}=10^9$ cells mL^{-1}) [28,37].

2.6. Antibacterial in LB medium

The minimum inhibition concentration (MIC) test was performed as follows. A series of as-prepared GO–AgNPs solutions with desired concentrations were added into 20 mL LB medium containing 10^6 colony-forming units per milliliter (CFU mL^{-1}). AgNPs solutions with same Ag content as GO–AgNPs and water were used as positive and negative control, respectively. The lowest concentration at which OD_{600} remains less than 0.1 was taken as the MIC value after 24 h incubation at 37 °C. All concentrations of GO–AgNPs and AgNPs are in terms of Ag.

2.7. Baird-Parker agar plate culture

LB medium containing agar base (20 g L^{-1}) was treated by autoclaving process firstly. After cooling down to about 50 °C, the agar solutions were mixed with GO–AgNPs or AgNPs and the mixtures were poured into culture dish (7.5 cm in diameter). After cooled down to room temperature, 100 μL of bacterial samples were spread on the agar-gel medium and cultured at 37 °C for 24 h.

3. Results and discussion

3.1. Synthesis and characterization of GO–AgNPs

The overall procedure of assembly is shown in Scheme 1. Firstly, poly(diallyldimethylammonium chloride) (PDDA) was introduced to be adsorbed on the GO sheets via electrostatic interaction between positive charged PDDA chain and negatively charged GO [38–40], which converted the zeta potential of GO from −39.0 mV to +38.2 mV (Table S1). PDDA-functionalized GO sheets (GO–PDDA) with distributed surface positive charges favor electrostatic self-assembly of negatively charged AgNPs (−40.1 mV) onto GO–PDDA [41]. As shown in Fig. 1a, 14 nm of AgNPs assembled both on the plane and at the edge of GO sheet homogeneous via electrostatic interactions.

Absorption spectra were used to investigate the conjugation of AgNPs and GO sheets. Fig. S1(a) shows the absorption spectra of GO, GO–PDDA, GO–AgNPs and AgNPs. The surface plasma resonance (SPR) absorption peak of AgNPs was at 396 nm with full width at half maximum (FWHM) of 55 nm. Compared with AgNPs, the absorbance band of GO–AgNPs was broadened (FWHM of 89 nm) and the peak red-shifted from 396 to 401 nm, which was due to the overlap of the dipole resonances between neighboring AgNPs [42,43]. In addition, the anchor of AgNPs on GO sheets ensured AgNPs colloidal stability in physiological solution and under ambient light. For comparison, the colloidal stabilities of AgNPs and GO–AgNPs were tested by light irradiation and high ionic strength solution incubation. As shown in Fig. S2(a), the color of AgNPs colloidal solution gradually changed from yellow to dark brown under ambient light within 5 days. Corresponding UV–vis spectra also showed that the maximum absorption peak of AgNPs was red-shifted from 396 nm to 403 nm with a significant decrease in absorbance. In addition, the color of AgNPs solution became poor gray and the characteristic SPR peak of AgNPs at 396 nm disappeared when AgNPs were just dispersed in PBS (as shown in Fig. S2(c)). The experimental results suggest that AgNPs easily form aggregates under light irradiation or high ionic strength. GO–AgNPs showed just little changes of both UV–vis spectra and solution color (as shown in Figs. S2(b) and (d)). The experimental result indicates that colloidal stability of AgNPs is strongly increased by anchored onto GO sheets. The phenomenon can be ascribed that the GO–PDDA substrate prevented aggregation of the anchored AgNPs.

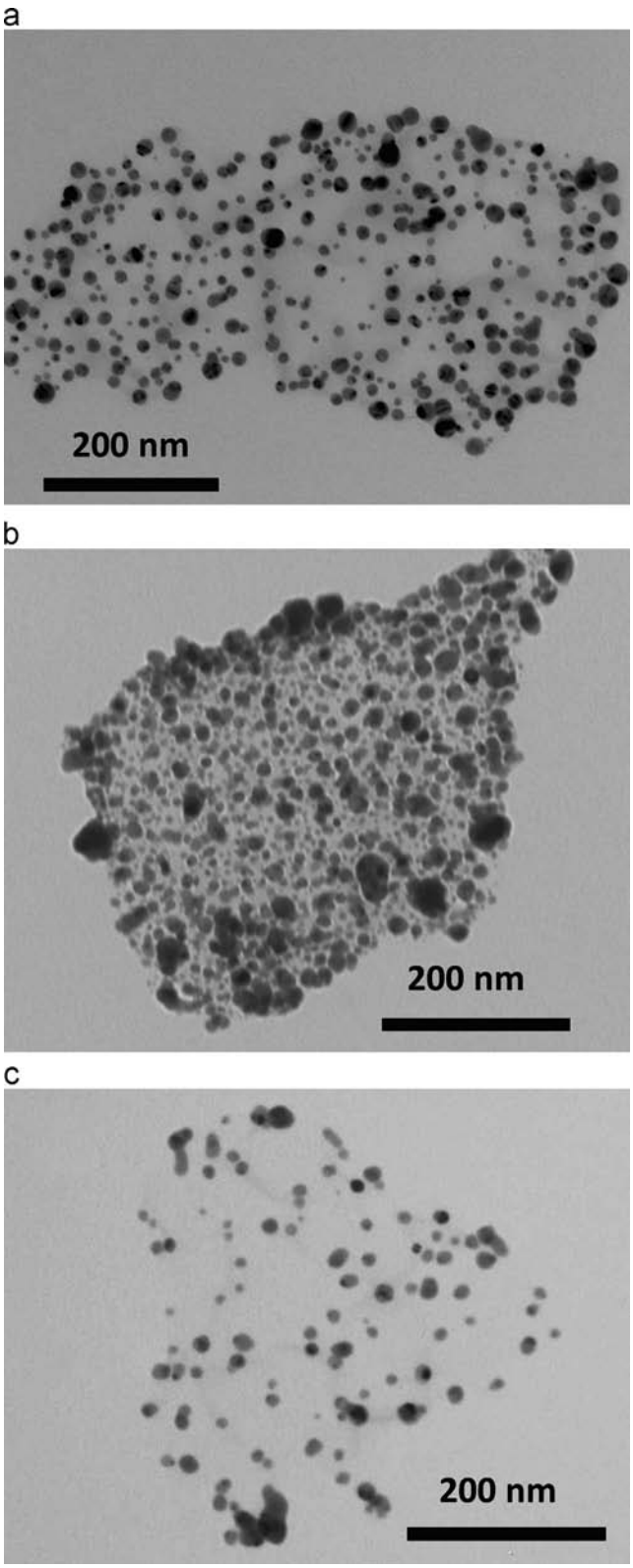

Fig. 1. TEM images of GO–AgNPs with different mass ratios of Ag to GO–PDDA, (a) for 2:1, (b) for 6:1 and (c) for 2:3, respectively.

Fig. 2(a) shows the FTIR spectra of GO, PDDA, GO–PDDA and GO–AgNPs. The spectrum of GO–PDDA shows new absorbance at 1418

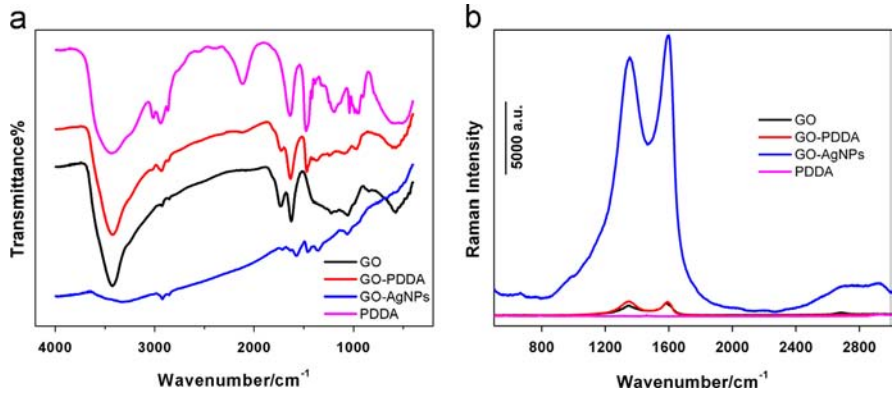

Fig. 2. FTIR (a) and Raman (b) spectra of GO, GO–PDDA, GO–AgNPs and PDDA, respectively. (For interpretation of the references to color in this figure, the reader is referred to the web version of this article.)

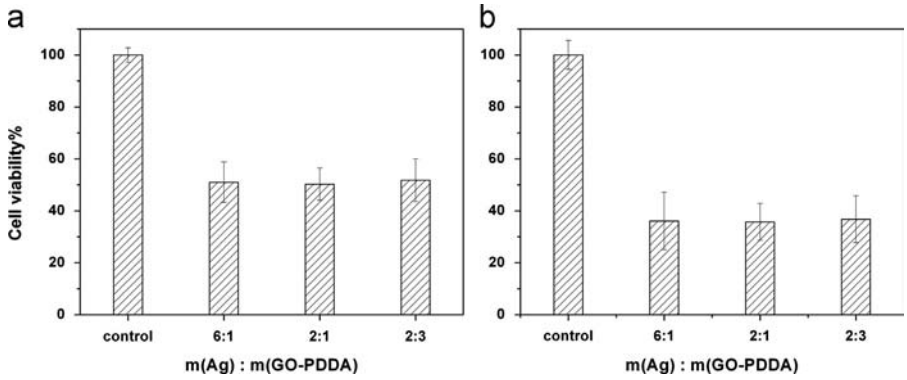

Fig. 3. Antibacterial activity of GO–AgNPs against *E. coli* (a) and *B. subtilis* (b). The mass ratio of AgNPs and GO–PDDA in the reaction mixtures are 6:1, 2:1 and 2:3, respectively. The concentrations of Ag are 2.4 μg mL^{-1} for (a) and 4.8 μg mL^{-1} for (b).

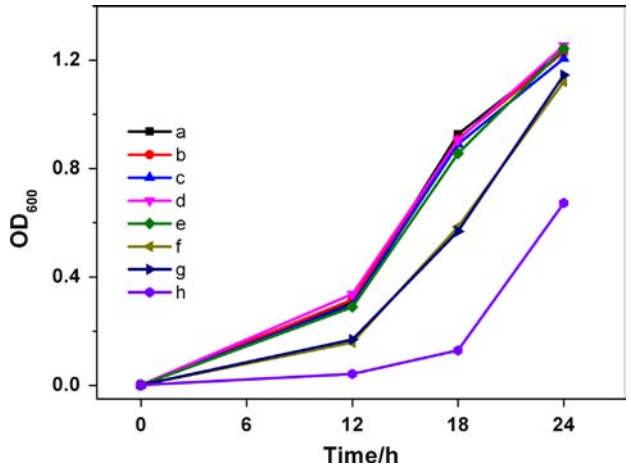

Fig. 4. *E. coli* growth curve in LB media containing 100 μL water (a), (b) to (e) for 1.6, 5, 10, 20 μg mL^{-1} GO–PDDA, (f) for 2.4 μg•mL^{-1} AgNPs, (g) for mixture of 2.4 μg mL^{-1} Ag and 1.2 μg mL^{-1} GO–PDDA, and (h) for 2.4 μg mL^{-1} GO–AgNPs, respectively.

and 1472 cm^{-1} due to the C–N stretching vibration of PDDA, and absorbance at 3015 cm^{-1} is ascribed to C3H stretching vibration of PDDA (pink curve) [44]. The intensity of C=O stretching peak at 1730 cm^{-1} of GO–PDDA (red curve) is decreased because the interaction of GO with PDDA leads to less C=O group exposed on the surface. As shown in Fig. 2(b), the Raman bands at 1393, 1595, 2700 and 2920 cm^{-1} of GO–AgNPs with strong intensity are assigned to D, G, 2D and S3 band of GO [45]. Furthermore, surface enhanced Raman scattering (SERS) intensity of GO–AgNPs dependent on the surface coverage of AgNPs on GO sheet can be obtained (as shown in the Fig. S4). The signal intensity enhancement which is derived from SERS effect of AgNPs [41,46,47]. X-ray photoelectron spectroscopy (XPS), a surface-sensitive technique, was used to analyze the chemical composition of GO-based materials. The XPS spectra of the GO, GO–PDDA and GO–AgNPs are shown in Fig. S3. The peak area ratio of C 1s (285 eV) and O 1 s (531.8 eV) of GO is 0.745, while the peak area ratio of C 1s and O 1s of GO–PDDA increased to 1.05. The results suggest that PDDA are adsorbed on the GO sheets. In addition, Cl 2p, Cl 2s and N 1s peak centered at 197, 268 and 402 eV also presented in GO–PDDA and GO–AgNPs [48–50]. The spectrum of GO–AgNPs shows 4 peaks at 367.80, 373.80, 573.6 and 604.0 eV, which are corresponding to Ag $3d_{5/2}$, Ag $3d_{3/2}$, Ag 3p3 and Ag 3p1 binding energy, respectively [51,52]. These results indicated that GO–AgNPs have been prepared successfully.

The thermogravimetric analysis (TGA) of GO–AgNPs and GO–PDDA, as shown in Fig. S5(a), displays the weight loss of samples. The weight loss of GO–PDDA (red trace) at temperatures of 150–190 °C could be ascribed to the decomposition of PDDA [22]. The large weight loss at 480–540 °C could be attributed to the bulk pyrolysis of graphene skeleton [30]. For GO–AgNPs, less weight loss is observed at these temperatures, and this result shows that as-synthesized GO–AgNPs contained 67.6 wt% silver.

Furthermore, the density of AgNPs on GO sheets can be simply tuned by varying the dosage of AgNPs added into GO–PDDA dispersions. With increasing mass ratio of AgNPs to GO–PDDA, the absorbance peak of GO–AgNPs around 400 nm dropped dramatically and the FWHM increased from 66 to 193 nm, as shown in Fig. S1(b), which is ascribed to decreased distance between neighboring AgNPs [42,43]. The phenomenon is also confirmed by TEM measurement. As shown in Fig. 1, when larger amount of AgNPs added into the reaction mixture, higher density of AgNPs on GO sheets can be obtained, and the distances among AgNPs are decreased. Moreover, different sizes

and shapes of AgNPs could also be conjugated on GO sheets by this approach. As shown in Fig. S6, large (46 ± 8.6 nm) AgNPs and Ag nanoplates (22 ± 6.5 nm in diameter) were anchored on the GO sheets successfully.

3.2. Antibacterial tests

Gram negative (G−) bacterial strain *E. coli* and Gram positive (G+) bacterial strain *B. subtilis* were chosen as the model organisms for addressing antibacterial activity of the GO–AgNPs.

3.2.1. Effect of the size of AgNPs

It has been reported that the antibacterial activity of AgNP-based materials is dependent on the size of AgNPs [53,54]. In this case, the AgNPs with average sizes of 14 (small) and 46 nm (large) in diameter were used to prepare the GO–AgNPs, respectively. The as-prepared nanohybrids were named as GO–AgNPs (small) and GO–AgNPs (large), respectively. As shown in Fig. S5(b), GO–AgNPs (small) exhibits much higher antibacterial activity than that of GO–AgNPs (large). This result is in agreement with previous reports that small AgNPs showed better antibacterial activities than that of the large AgNPs [55,56]. Therefore, 14 nm AgNPs conjugated GO were used in following experiments.

3.2.2. Effect of AgNPs density on GO sheets

GO–AgNPs with different mass ratios (6:1, 2:1 and 2:3 of Ag to GO–PDDA) have been prepared to evaluate the antibacterial properties of the GO–AgNPs nanocomposites with different AgNPs densities. In this case, two kinds of bacteria strains (*E. coli* and *B. subtilis*) were used. A certain concentration of GO–AgNPs was added to the conical flask containing 20 mL LB medium with the final bacterial concentration of 10^6 CFU mL^{-1}. As shown in Fig. 3, same bacterial inhibitions were found against both *E. coli* (a) and *B. subtilis* (b). As negative control, GO–PDDA with different concentrations shows negligible antibacterial capacity (as shown in Fig. 4). It is confirmed that the amount of silver is the crucial factor to effect on the antibacterial performance of GO–AgNPs. This finding was different to previously reported result [26], which might be due to different preparing procedures of GO–AgNPs. The hybrids with Ag to GO–PDDA mass ratio of 2:1 were used in following work.

3.2.3. Bacterial inhibition test of GO–AgNPs vs. AgNPs

The bacterial inhibition growth curve was used to study different antibacterial efficacy of AgNPs and GO–AgNPs through the growth kinetics of two kinds of strains (*E. coli* and *B. subtilis*) cultured with a series of concentrations of GO–AgNPs or AgNPs. The bacterial growth curves are shown in Fig. 5. The results demonstrate that after 24 h germiculture, for *E. coli* (as shown in Fig. 5(b)), the MIC of GO–AgNPs and AgNPs are 3.2 μg mL^{-1} and 6.4 μg mL^{-1}, respectively. Moreover, GO–AgNPs shows longer-termed efficacy than that of AgNPs (as shown in Fig. 5(a)). For *B. subtilis*, GO–AgNPs also showed better antibacterial efficacy than that of AgNPs (as shown in Fig. 5(c)). Towards to *B. subtilis*, the MICs of GO–AgNPs and AgNPs are 6.4 μg mL^{-1} and 9.6 μg mL^{-1}, respectively (Fig. 5(d)).

These different susceptibilities to Ag-based materials between *B. subtilis* and *E. coli* were consistent with previous reports [26]. This may due to different cell wall structures and different

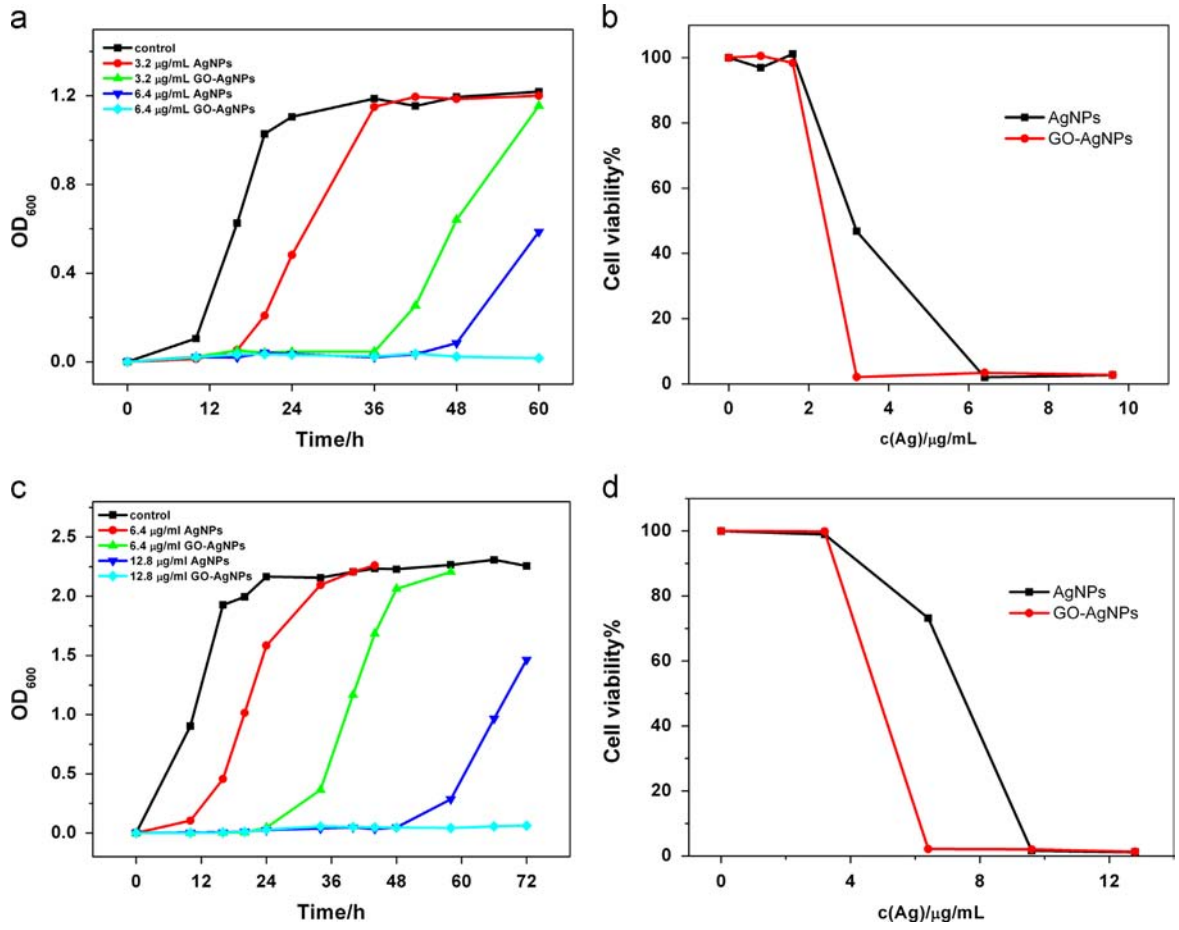

Fig. 5. Bacterial growth curve in LB media. (a) and (b) for *E. coli*, (c) and (d) for *B. subtilis*. (b) and (d) for strains incubated with different concentrations of AgNPs or GO–AgNPs for 24 h, respectively.

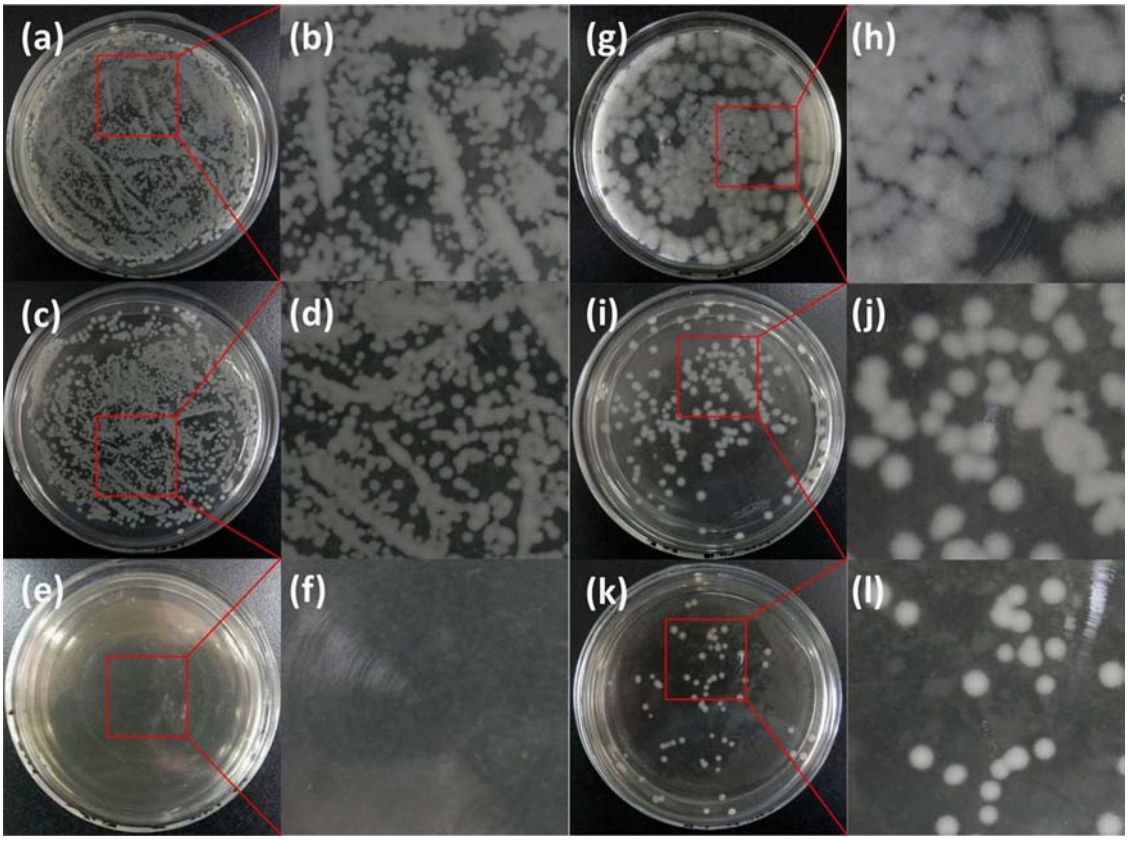

Fig. 6. LB-agar plate tests against *E. coli* cells (a–f) and *B. subtilis* (g–l). (a), (b), (g) and (h) for control, (c), (d), (i) and (j) for LB-agar containing AgNPs, (e), (f), (k) and (l) for LB-agar containing GO–AgNPs. (b), (d), (f), (h), (j) and (l) for enlarged images of (a), (c), (e), (g), (i) and (k). The concentrations of Ag for *E. coli* and *B. subtilis* are 3.2 and 6.4 μg mL^{-1}, respectively.

antibacterial mechanisms of Ag against different cells [55,57]. For instance, G− bacteria possess a thin peptidoglycon layer (7–8 nm thickness), whereas G+ bacteria possess a thick peptidoglycon layer (about 20–80 nm thickness) [58], which are more resistant to Ag^+ diffusion.

Then either the enhanced antibacterial effect of GO–AgNPs hybrids could be ascribed to the synergistic effect of AgNPs and GO–PDDA or just an additive effect of AgNPs and GO–PDDA. To address this problem, *E. coli* cells were incubated in LB medium with GO–PDDA, AgNPs, GO–AgNPs and successively addition of GO and AgNPs, respectively (the amount of GO–PDDA and AgNPs were equal in this section, respectively). As shown in Fig. 4, GO–PDDA (line b) shows no growth inhibition ability at all, and the mixture of GO–PDDA and AgNPs (line g) shows no enhanced antibacterial activity compared with that of AgNPs (line f), both of which are much weaker than that of GO–AgNPs. Therefore, this enhanced antibacterial activity of GO–AgNPs is not due to the additive effect of AgNPs and GO–PDDA but due to the synergistic effect of AgNPs and GO–PDDA.

The high stability of the GO–AgNPs nanostructures is responsible for their high and long-term antibacterial activity. Electrostatic interaction of bacterial and GO–AgNPs gives further promote the antibacterial activity of GO–AgNPs, because the bacteria are negatively charged at biological pH values due to the dissociation of an excess number of carboxylic and other groups in the membrane [25,59]. Therefore, the electrostatic interactions between the strain cells and the GO–AgNPs (+20.3 mV, Table S1) would be facilitated in an aqueous solution.

The results from the colony forming count method of LB-agar experiment are given in Fig. 6, which are in good agreement with the results obtained from LB medium assay. For *E. coli*, the colonies were totally inhibited when incubated on GO–AgNPs stained LB-agar (Fig. 6(e) and (f)), while lots number of colonies can be seen on AgNPs stained LB-agar. The number of *B. subtilis* colonies on GO–AgNPs stained LB-agar is about one third of that on AgNPs stained LB-agar. Therefore, GO–AgNPs show much higher antibacterial activity than that of AgNPs both in LB medium and on LB-agar culture.

4. Conclusions

GO–AgNPs was prepared by a simple strategy based on electrostatic interactions between oppositely charged GO–PDDA and AgNPs. This strategy allows AgNPs of various morphologies to be easily attached onto GO, which provides a simple and general method to prepare GO–metal NPs composites. The GO–AgNPs exhibits much higher stability both in saline solution and under ambient light irradiation than that of colloidal AgNPs. The antibacterial activities of GO–AgNPs were found to be enhanced more than one times compared to that of AgNPs against both G− *E. coli* and G+ *B. subtilis*. The high stability, positive charged surface and enhanced antibacterial properties of GO–AgNPs promote further use of hybrids as a powerful antibacterial agent in industrial and clinical applications.

Acknowledgments

This research was supported by National Basic Research Program of China (Grant no. 2011CB935800).

Appendix A. Supplementary material

Supplementary data associated with this article can be found in the online version at http://dx.doi.org/10.1016/j.talanta.2013.09.017.

References

[1] S.G. Berk, J.H. Gunderson, A.L. Newsome, A.L. Farone, B.J. Hayes, K.S. Redding, N. Uddin, E.L. Williams, R.A. Johnson, M. Farsian, A. Reid, J. Skimmyhorn, M. B. Farone, Environ. Sci. Technol. 40 (2006) 7440–7444.
[2] Y.-F. Huang, Y.-F. Wang, X.-P. Yan, Environ. Sci. Technol. 44 (2010) 7908–7913.
[3] S. Lin, Z. Zhang, H. Xu, L. Li, S. Chen, J. Li, Z. Hao, P.R. Chen, J. Am. Chem. Soc. 133 (2011) 20581–20587.
[4] M.E. Dueker, G.D. O'Mullan, A.R. Juhl, K.C. Weathers, M. Uriarte, Environ. Sci. Technol. 46 (2012) 10926–10933.
[5] H. Bai, Z. Liu, D.D. Sun, Phys. Chem. Chem. Phys. 13 (2011) 6205–6210.
[6] X. Liang, M. Sun, L. Li, R. Qiao, K. Chen, Q. Xiao, F. Xu, Dalton Trans. 41 (2012) 2804–2811.
[7] S. Liu, T.H. Zeng, M. Hofmann, E. Burcombe, J. Wei, R. Jiang, J. Kong, Y. Chen, ACS Nano 5 (2011) 6971–6980.
[8] S. Liu, M. Hu, T.H. Zeng, R. Wu, R. Jiang, J. Wei, L. Wang, J. Kong, Y. Chen, Langmuir 28 (2012) 12364–12372.
[9] A. Taglietti, Y.A. Diaz Fernandez, E. Amato, L. Cucca, G. Dacarro, P. Grisoli, V. Necchi, P. Pallavicini, L. Pasotti, M. Patrini, Langmuir 28 (2012) 8140–8148.
[10] P. Sanpui, A. Murugadoss, P.V. Prasad, S.S. Ghosh, A. Chattopadhyay, Int. J. Food Microbiol. 124 (2008) 142–146.
[11] J. Cui, C. Hu, Y. Yang, Y. Wu, L. Yang, Y. Wang, Y. Liu, Z. Jiang, J. Mater. Chem. 22 (2012) 8121–8126.
[12] M. Rai, A. Yadav, A. Gade, Biotechnol. Adv. 27 (2009) 76–83.
[13] E. Navarro, F. Piccapietra, B. Wagner, F. Marconi, R. Kaegi, N. Odzak, L. Sigg, R. Behra, Environ. Sci. Technol. 42 (2008) 8959–8964.
[14] C.-N. Lok, C.-M. Ho, R. Chen, Q.-Y. He, W.-Y. Yu, H. Sun, P.-H. Tam, J.-F. Chiu, C.-M. Che, J. Biol. Inorg. Chem. 12 (2007) 527–534.
[15] H. Kong, J. Jang, Langmuir 24 (2008) 2051–2056.
[16] M. Lv, S. Su, Y. He, Q. Huang, W. Hu, D. Li, C. Fan, S.T. Lee, Adv. Mater. 22 (2010) 5463–5467.
[17] H. Yang, Y. Liu, Q. Shen, L. Chen, W. You, X. Wang, J. Sheng, J. Mater. Chem. 22 (2012) 24132–24138.
[18] H. Zhang, G. Grüner, Y. Zhao, J. Mater. Chem. B 1 (2013) 2542–2567.
[19] S. Guo, S. Dong, Chem. Soc. Rev. 40 (2011) 2644–2672.
[20] J. Liu, S. Fu, B. Yuan, Y. Li, Z. Deng, J. Am. Chem. Soc. 132 (2010) 7279–7281.
[21] S. Guo, S. Sun, J. Am. Chem. Soc. 134 (2012) 2492–2495.
[22] Y. Fang, S. Guo, C. Zhu, Y. Zhai, E. Wang, Langmuir 26 (2010) 11277–11282.
[23] Z. Zhu, L. Ma, M. Su, D. Liu, Z. Wang, J. Mater. Chem. B 1 (2013) 1432.
[24] C. Li, X. Wang, F. Chen, C. Zhang, X. Zhi, K. Wang, D. Cui, Biomaterials 34 (2013) 3882–3890.
[25] J. Ma, J. Zhang, Z. Xiong, Y. Yong, X.S. Zhao, J. Mater. Chem. 21 (2011) 3350.
[26] J. Tang, Q. Chen, L. Xu, S. Zhang, L. Feng, L. Cheng, H. Xu, Z. Liu, R. Peng, ACS Appl. Mater. Interfaces 5 (2013) 3867–3874.
[27] Z. Zhang, J. Zhang, B. Zhang, J. Tang, Nanoscale 5 (2013) 118–123.
[28] Y. Zhou, J. Yang, T. He, H. Shi, X. Cheng, Y. Lu, Small (2013), http://dx.doi.org/10.1002/smll.201202455.
[29] L. Liu, J. Liu, Y. Wang, X. Yan, D.D. Sun, N. J. Chem. 35 (2011) 1418.
[30] C. Zhu, S. Guo, Y. Fang, S. Dong, ACS Nano 4 (2010) 2429–2437.
[31] W.S. Hummers, R.E. Offeman, J. Am. Chem. Soc. 80 (1958) 1339.
[32] Y. Qin, X. Ji, J. Jing, H. Liu, H. Wu, W. Yang, Colloids Surf. A 372 (2010) 172–176.
[33] H. Li, H. Xia, D. Wang, X. Tao, Langmuir 29 (2013) 5074–5079.
[34] Q. Zhang, N. Li, J. Goebl, Z. Lu, Y. Yin, J. Am. Chem. Soc. 133 (2011) 18931–18939.
[35] M.-C. Wu, A.R. Deokar, J.-H. Liao, P.-Y. Shih, Y.-C. Ling, ACS Nano 7 (2013) 1281–1290.
[36] J. Wang, J. Gao, D. Liu, D. Han, Z. Wang, Nanoscale 4 (2012) 451–454.
[37] E. Amato, Y.A. Diaz-Fernandez, A. Taglietti, P. Pallavicini, L. Pasotti, L. Cucca, C. Milanese, P. Grisoli, C. Dacarro, J.M. Fernandez-Hechavarria, V. Necchi, Langmuir 27 (2011) 9165–9173.
[38] X. Wang, J. Wang, H. Cheng, P. Yu, J. Ye, L. Mao, Langmuir 27 (2011) 11180–11186.
[39] X. Dong, L. Wang, D. Wang, C. Li, J. Jin, Langmuir 28 (2011) 293–298.
[40] Y.H. Lee, L. Polavarapu, N. Gao, P. Yuan, Q.H. Xu, Langmuir 28 (2012) 321–326.
[41] W. Ren, Y. Fang, E. Wang, ACS Nano 5 (2011) 6425–6433.
[42] S. Mandal, A. Gole, N. Lala, R. Gonnade, V. Ganvir, M. Sastry, Langmuir 17 (2001) 6262–6268.
[43] A.D. McFarland, R.P. Van Duyne, Nano Lett. 3 (2003) 1057–1062.
[44] D.-Q. Yang, J.-F. Rochette, E. Sacher, J. Phys. Chem. B 109 (2005) 4481–4484.
[45] T.V. Cuong, V.H. Pham, Q.T. Tran, S.H. Hahn, J.S. Chung, E.W. Shin, E.J. Kim, Mater. Lett. 64 (2010) 399–401.
[46] L. Sun, D. Zhao, M. Ding, Z. Xu, Z. Zhang, B. Li, D. Shen, J. Phys. Chem. C 115 (2011) 16295–16304.
[47] Y.Q. Wang, S. Ma, Q.Q. Yang, X.J. Li, Appl. Surf. Sci. 258 (2012) 5881–5885.
[48] K. Kanamura, S. Shiraishi, H. Takezawa, Z.-i. Takehara, Chem. Mater. 9 (1997) 1797–1804.
[49] T. Ramanathan, F.T. Fisher, R.S. Ruoff, L.C. Brinson, Chem. Mater. 17 (2005) 1290–1295.
[50] Y.J. Kim, C.R. Park, Inorg. Chem. 41 (2002) 6211–6216.
[51] A. Melaiye, R.S. Simons, A. Milsted, F. Pingitore, C. Wesdemiotis, C.A. Tessier, W.J. Youngs, J. Med. Chem. 47 (2004) 973–977.
[52] J. Song, H. Kang, C. Lee, S.H. Hwang, J. Jang, ACS Appl. Mater. Interfaces 4 (2012) 460–465.
[53] G.A. Sotiriou, S.E. Pratsinis, Environ. Sci. Technol. 44 (2010) 5649–5654.
[54] J.R. Morones, J.L. Elechiguerra, A. Camacho, K. Holt, J.B. Kouri, J.T. Ramírez, M. J. Yacaman, Nanotechnology 16 (2005) 2346.
[55] X. Jin, M. Li, J. Wang, C. Marambio-Jones, F. Peng, X. Huang, R. Damoiseaux, E. M.V. Hoek, Environ. Sci. Technol. 44 (2010) 7321–7328.
[56] G.A. Martínez-Castañón, N. Niño-Martínez, F. Martínez-Gutierrez, J. R. Martínez-Mendoza, F. Ruiz, J. Nanopart. Res. 10 (2008) 1343–1348.
[57] M. Banerjee, S. Sharma, A. Chattopadhyay, S.S. Ghosh, Nanoscale 3 (2011) 5120–5125.
[58] A. Kumar, P.K. Vemula, P.M. Ajayan, G. John, Nat. Mater. 7 (2008) 236–241.
[59] P.K. Stoimenov, R.L. Klinger, G.L. Marchin, K.J. Klabunde, Langmuir 18 (2002) 6679–6686.